Chinese Chemical Letters 31 (2020) 1648–1653

Contents lists available at ScienceDirect

Chinese Chemical Letters

journal homepage: www.elsevier.com/locate/cclet

Communication

Functional groups to modify g-C_3N_4 for improved photocatalytic activity of hydrogen evolution from water splitting

Fan Yu[a], Laichun Wang[a], Qiuju Xing[a], Dengke Wang[a], Xunheng Jiang[a], Guangchao Li[b], Anmin Zheng[b], Fanrong Ai[c,*], Jian-Ping Zou[a,*]

[a] Key Laboratory of Jiangxi Province for Persistent Pollutants Control and Resources Recycle, Nanchang Hangkong University, Nanchang 330063, China
[b] State Key Laboratory of Magnetic Resonance and Atomic and Molecular Physics, National Center for Magnetic Resonance in Wuhan, Wuhan Institute of Physics and Mathematics, Chinese Academy of Sciences, Wuhan 430071, China
[c] School of Mechanical & Electronic Engineering, Nanchang University, Nanchang 330031, China

ARTICLE INFO

Article history:
Received 25 June 2019
Received in revised form 22 July 2019
Accepted 24 July 2019
Available online 15 August 2019

Keywords:
Functional groups
Graphitic carbon nitride
Hydrogen evolution
Photocatalysis
Synthesis

ABSTRACT

Rational modification by functional groups was regarded as one of efficient methods to improve the photocatalytic performance of graphitic carbon nitride (g-C_3N_4). Herein, g-C_3N_4 with yellow (Y-GCN) and brown (C-GCN) were prepared by using the fresh urea and the urea kept for five years, respectively, for the first time. Experimental results show that the H_2 production rate of the C-GCN is 39.06 μmol/h, which is about 5 times of the Y-GCN. Meantime, in terms of apparent quantum efficiency (AQE) at 420 nm, C-GCN has a value of 6.3% and nearly 7.3 times higher than that of Y-GCN (0.86%). The results of XRD, IR, DRS, and NMR show, different from Y-GCN, a new kind of functional group of —N=CH— was firstly *in-situ* introduced into the C-GCN, resulting in good visible light absorption, and then markedly improving the photocatalytic performance. DFT calculation also confirms the effect of the —N=CH— group band structure of g-C_3N_4. Furthermore, XPS results demonstrate that the existence of —N=CH— groups in C-GCN results in tight interaction between C-GCN and Pt nanoparticles, and then improves the charge separation and photocatalytic performance. The present work demonstrates a good example of "defect engineering" to modify the intrinsic molecular structure of g-C_3N_4 and provides a new avenue to enhance the photocatalytic activity of g-C_3N_4 *via* facile and environmental-friendly method.

Photocatalytic hydrogen evolution from water is one of the most promising green technology for direct conversion of solar energy to chemical energy and energy storage. In the past few decades, it has attracted immense efforts for developing various photocatalysts to produce H_2 through solar water splitting [1–4]. Recently, graphitic carbon nitride (g-C_3N_4), a metal-free photocatalyst, has received extensive attention due to its good photocatalytic hydrogen and oxygen production of water splitting [5–7], water oxidation [8,9], photocatalytic degradation of organic pollutants [10–12], organic reaction catalyst [13,14], catalyst carrier and energy storage material [15–17].

Currently, tremendous efforts have been focused on reporting synthesis of g-C_3N_4 by thermal treatment of different nitrogen-rich precursors under different reaction conditions [18–20]. For example, Martin research group reported that g-C_3N_4 can be prepared by using different precursors such as urea, melamine or dicyandiamide under same high-temperature calcination and ambient atmosphere conditions [21–26]. Subsequent reports on large amounts of urea-derived g-C_3N_4 outperformed the thiourea- and dicyandiamide-derived counterparts in the photocatalytic hydrogen evolution from water splitting [27,28]. Large numbers of refreshing literatures have reported on the effect of calcination temperature and precursor treatment on the synthesis, structure and properties of the g-C_3N_4 [29,30]. These reports indicated that different precursor and its reaction conditions of high-temperature calcination, ambient atmosphere and special precursor treatment methods can affect the physicochemical properties of g-C_3N_4, such as specific surface area, light absorption edge and nanostructures [31–33]. However, these literatures did not involve the influence of the preservation time and morphology of the same precursor on the thermal polymerization method, structure and photocatalytic property of g-C_3N_4.

In addition, many modification strategies have been reported to improve the photocatalytic performance of g-C_3N_4, including alkali-assisted synthesis, phosphorous-mediated synthesis and

* Corresponding authors.
E-mail addresses: afr3755875@126.com (F. Ai), zjp_112@126.com (J.-P. Zou).

https://doi.org/10.1016/j.cclet.2019.08.020
1001-8417/

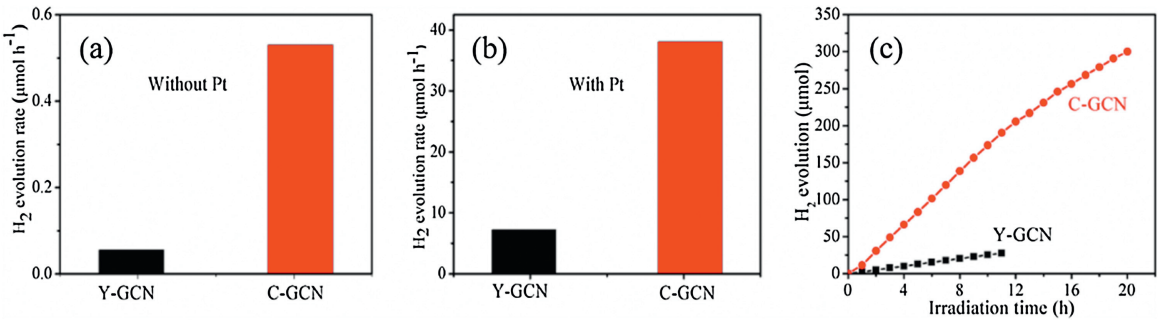

Fig. 1. (a) Hydrogen evolution rate to Y-GCN and C-GCN without Pt in 80 mL of aqueous solution under visible-light irradiation. (b) Pt-loaded Y-GCN and C-GCN photocatalysts in aqueous solution under visible-light irradiation. (c) Time course of hydrogen evolution over 20 h for C-GCNand Y-GCN.

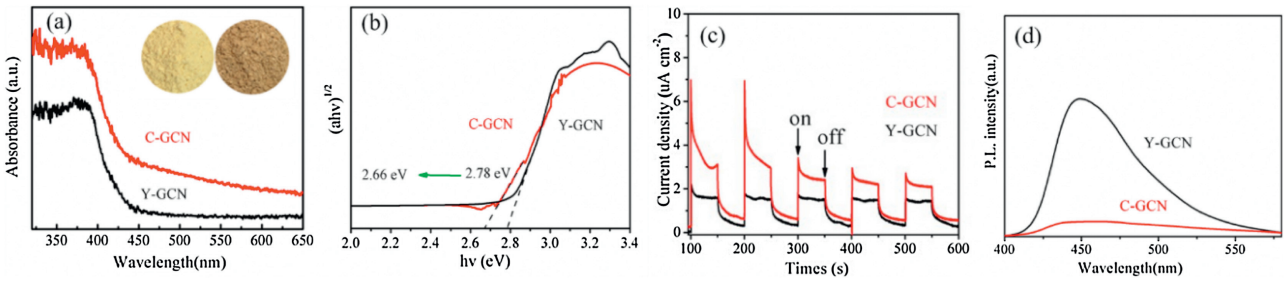

Fig. 2. (a) DRS and (b) plots of $(ahv)^2$ *vs.* hv over the Y-GCN and C-GCN (Inset in (a) shows a digital photograph of Y-GCN and C-GCN). (c) Transient photocurrent response of Y-GCN and C-GCN under visible-light illumination. (d) Photoluminescence spectra of Y-GCN and C-GCN at an excitation wavelength of 375 nm.

acid pretreatment of the precursors [34–36]. These strategies can generate functional groups (such as —OH, —COOH, —C≡N and $-CONH_2$) *via* defects formation to increase active sites, enhance light absorption and change the electronic band structure of g-C_3N_4. For example, —C≡N can be formed in the g-C_3N_4 by alkali-assisted synthesis to improve the photocatalytic performance of g-C_3N_4 [37]. In addition, $-CONH_2$ can be formed in the g-C_3N_4 by acid pretreatment to improve the photocatalytic performance of g-C_3N_4 [38]. However, these strategies are not environmental-friendly, complex and expensive because they need supply additives or special auxiliary conditions during the synthetic process and result in environmental pollution, such as usage of strong acid and formation of H_2S. Therefore, it is urgent to develop a facile and environmental-friendly approach for in-situ formation functional groups or defects in the g-C_3N_4 *via* direct calcination of N-rich precursors, thereby improve the photocatalytic performance of g-C_3N_4.

Herein, we tried to synthesize g-C_3N_4 with functional groups by calcination of the same precursorwith different kept-time. When the fresh urea and the urea kept for five years were used as precursors, it can obtain g-C_3N_4 with different color and photo-catalytic activity. The g-C_3N_4 obtained from the fresh urea and the urea kept for five years are yellow and brown, respectively, and they are hereafter named as Y-GCN and C-GCN, respectively. Noteworthily, C-GCN exhibits more than 5 times higher photo-catalytic H_2 generation rate than that of Y-GCN. We systematically investigated the structures, morphologies, and the hydrogen evolution properties of Y-GCN and C-GCN. Experimental results show that a new kind of functional group of —N=CH— was firstly introduced into the C-GCN, resulting in enhancement of visible light absorption and variation of band structure and improvement of charge carrier separation. The present work not only provides a new idea to prepare g-C_3N_4 with special defects but also demonstrates the introduction of —N=CH— groups into g-C_3N_4 is an effective approach of "defect engineering" to improve the photocatalytic performance of g-C_3N_4 for the first time.

The photocatalytic hydrogen evolution of C-GCN and Y-GCN were evaluated under irradiation of visible light using triethanol-amine as holes scavenger. As shown in Fig. 1a, in the absence of Pt co catalysts, the H_2 evolution rate of C-GCN is 26.5 μmol g^{-1} h^{-1}, which is about 10 times of Y-GCN (2.8 μmol g^{-1} h^{-1}). After loaded with Pt cocatalysts *via in situ* photo reduction of H_2PtCl_6, the H_2 evolution rates of C-GCN and Y-GCN are both greatly improved due to platinum's high conductivity, negligible over potential for H_2 evolution and excellent electron transport kinetic. As shown in Fig. 1b, the hydrogen evolution rate of C-GCN and Y-GCN is 1953 and 361.5 μmol g^{-1} h^{-1}, respectively, when Pt was loaded on the surface of catalysts. The H_2 evolution rates of C-GCN and Y-GCN nearly become nearly unchanged over 20 h photoreaction, indicating that they show good photo stability (Fig. 1c). In terms of apparent quantum efficiency (AQE) at 420 nm, C-GCN has a value of 6.3% and nearly 7.3 times higher than that of Y-GCN at 0.86%.

To explore the marked difference of the photocatalytic performance between C-GCN and Y-GCN, some tests were used. As shown in Fig. 2a, the C-GCN powder is gray, while Y-GCN is faint yellow. Compared with Y-GCN, C-GCN has much stronger absorption intensity in the visible light region and the absorption edge obviously red-shifts. As shown in Fig. 2b, the calculated bandgaps of Y-GCN and C-GCN are 2.78 eV and 2.66 eV, respectively. As shown in Fig. 2c, C-GCN exhibits much better photocurrent than Y-GCN. C-GCN shows lower intensity of PL spectra than Y-GCN (Fig. 2d). The above results indicate that C-GCN has much better light absorption and more efficient separation rate of photo generated electrons and holes than Y-GCN.

The crystal and molecular structure of Y-GCN and C-GCN were systematically researched in order to make clear their different photocatalytic performance. Fig. 3 shows the results of ^{13}C and ^{15}N MAS NMR of Y-GCN and C-GCN. The ^{13}C spectra of two samples show two resonance peaks at δ_1 165 ppm and δ_2 156.7 ppm (Fig. 3a). The peak at 165.4 ppm is ascribed to the C(2) atoms in

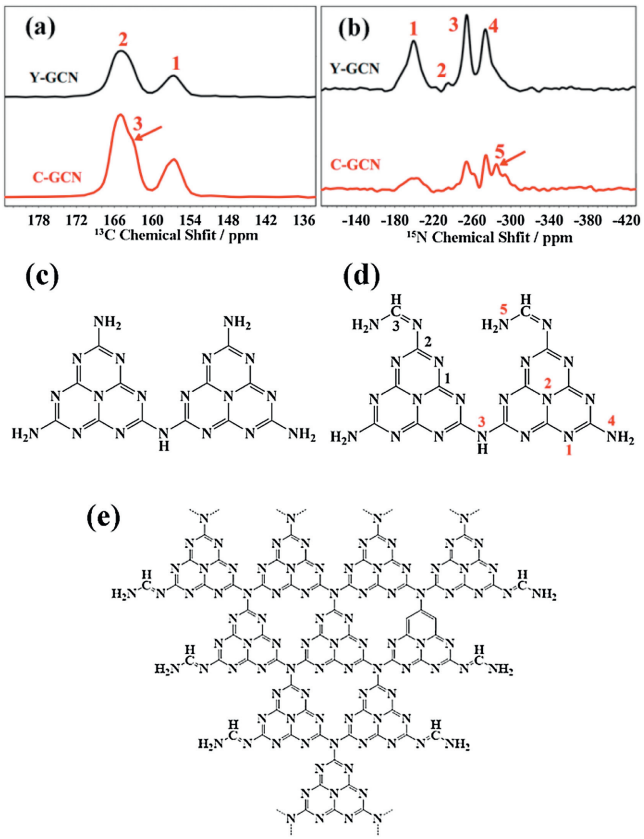

Fig. 3. (a) ^{13}C and (b) ^{15}N solid state NMR spectra of Y-GCN and C-GCN. (c) The molecular structure of Y-GCN and (d) C-GCN. (e) Network structure of C-GCN.

CN_2, while the peak at 156.7 ppm is assigned to C(1) atoms in CN_3 groups [39,40]. The results are well consistent with those reported by Wang et al, confirming the C-GCN possesses the g-C_3N_4 framework. In addition, a new signal at 163.4 ppm (C3) appears in the C-GCN, which can be ascribed to the imine signal, indicating that the peripheral —N=CH— groups exist in C-GCN [41]. Four peaks in the ^{15}N spectra of Y-GCN and C-GCN can be assigned (Fig. 3b). The broad signal at the –199.9 ppm corresponds to the peripheral nitrogens (N1) in the heptazine ring; the weak peak at –235.1 ppm is assigned to the center nitrogen (N2) of heptazine; the strongest peak at –254.2 ppm is attributed to the secondary amine (N3: -NH group); and the ^{15}N signal at –274 ppm is ascribed to amine (N4: -NH_2 group) [42,43]. The above four peaks coincide with those of g-C_3N_4, indicating the g-C_3N_4 structure exists in C-GCN and Y-GCN. In addition, a new signal at –285.4 ppm (N5) among the C-GCN coincides with the urea NH_2 signal, demonstrating a new peripheral amine groups were formed in C-GCN [38]. Compared to the structure of Y-GCN (Fig. 3c), the NMR results confirm the existence of peripheral —N=CH—NH_2 groups in C-GCN (Fig. 3d).

In addition, carbon and nitrogen contents of Y-GCN and C-GCN samples were determined by elemental analyses. As shown in Table 1, the C/N atomic ratio of Y-GCN and C-GCN is 0.668 and 0.695, respectively, lower than the theoretical value of 0.75 for g-C_3N_4, which could be due to the existence of many amino groups (C-NH_x) [27]. The larger C/N atomic ratio of C-GCN than that of Y-GCN also indicates the existence of peripheral —N=CH— group in the C-GCN. Furthermore, as shown in Table 1, the organic elemental analysis (OEA) shows the C/N atomic ratio of 0.695 for C-GCN is consistent with the calculated C/N atomic ratio (0.7) of the polymeric structure for the —N=CH—NH_2 group modified g-C_3N_4 (Fig. 3e). The result is consistent with the above analysis of NMR results.

Table 1
The physicochemical properties of Y-GCN and C-GCN.

Samples	C/N molar ratio		BET (m^2/g)	Pore size (nm)
	XPS	OEA		
Y-GCN	0.73	0.668	35.99	12.82
C-GCN	0.86	0.695	79.22	17.40

As shown in Fig. 4a, the XRD patterns of C-GCN are similar to that of Y-GCN. Two obvious featured peaks are found in Y-GCN and C-GCN. The weak peak at 12.9°, indexed as the (100) of g-C_3N_4, confirms that the tri-s-triazine-based structure is retained in C-GCN [19]. The strong peak at 27.8° is indexed as (002) of g-C_3N_4, which is ascribed to the interlayer stacking of conjugated aromatic rings [44]. Noteworthily, the (002) peak shifts from 27.8° of Y-GCN to 27.4° of C-GCN, suggesting that the crystal structure of the C-GCN tends to become less stable than Y-GCN [45]. Furthermore, there are two other weak peaks at 17.6 and 21.4 in the C-GCN, corresponding to (011) and (110) of g-C_3N_4 [46]. The results confirm that both Y-GCN and C-GCN show the structure of g-C_3N_4.

As shown in Fig. 4b, FT-IR spectrum of C-GCN is similar to that of Y-GCN. Among them, there are five characteristic peaks at 810, 1240, 1320, 1411, 1459, and 1638 cm^{-1}, which are attributed to the skeletal vibrations of tri-s-triazine ring units of g-C_3N_4 [47,48]. The peaks at 3170 cm^{-1} and 3277 cm^{-1} are ascribed to the stretching vibration of –NH_2 and –OH, respectively [49,50]. And the peak at 1565 cm^{-1} is assigned to the stretching vibration of N=C group [51,52]. Compared with the Y-GCN, the peak's intensity of N=C group markedly increase among the C-GCN. The above results indicate that the units of tri-s-triazine ring exist in the C-GCN and Y-GCN, and there could exist peripheral —N=C— group in the C-GCN.

The wide-scan XPS spectra of Y-GCN and C-GCN confirm the existence of C, N, and O elements in Y-GCN and C-GCN (Fig. S1 in Supporting information). As shown in Fig. 4c, there are three peaks at 288.26, 285.96 and 284.72 eV among Y-GCN and C-GCN, corresponding to N—C=N in the framework of g-C_3N_4, C-NH_x (x = 1 and 2) on the edges of heptazine units and adventitious hydrocarbons (C—C/C=C), respectively [53]. Noteworthily, compared with Y-GCN, C-NH_x signal exhibits a small shift to higher binding energy in C-GCN, which can be taken as good evidence for the formation of new defect group in C-GCN [54]. Furthermore, there is additional peak at 284.78 eV among the C1s spectra of C-GCN that is attributed to –C–H species, implying a new group of –C–H in C-GCN [55]. As shown in Fig. 4d, the N1 s spectra of Y-GCN and C-GCN can be deconvoluted into three peaks at 398.74, 399.76 and 401.2 eV, which can be ascribed to bi-coordinated (N_{2C}) and tri-coordinated (N_{3C}) nitrogen atoms and C-NH_x (x = 1 and 2) groups in the heptazine framework, respectively [56,57]. Compared with Y-GCN, the peaks of N_{2C} among C-GCN slightly shift to higher binding energy, which could be due to the generation of terminal —CH=N— groups whose N 1s binding energy are intermediate between those of N_{2C} and N_{3C} in C-GCN (Table S1 in Supporting information) [58]. These results are consistent with those reported in the literature. Furthermore, the elementary analysis based on XPS data shows that the C/N ratio increases from 0.73 in Y-GCN to 0.86 in the C-GCN (Table 1), confirming the existence of terminal group of —CH=N— in C-GCN. Therefore, based on the NMR, FTIR and XPS results, it can be concluded that the peripheral —N=CH—NH_2 groups appear in C-GCN but not in Y-GCN.

The morphologies of Y-GCN and C-GCN were investigated (Fig. 5). The Y-GCN and C-GCN consist of large amounts of packing layers with different sizes of nanosheets (Figs. 5a and b). As shown

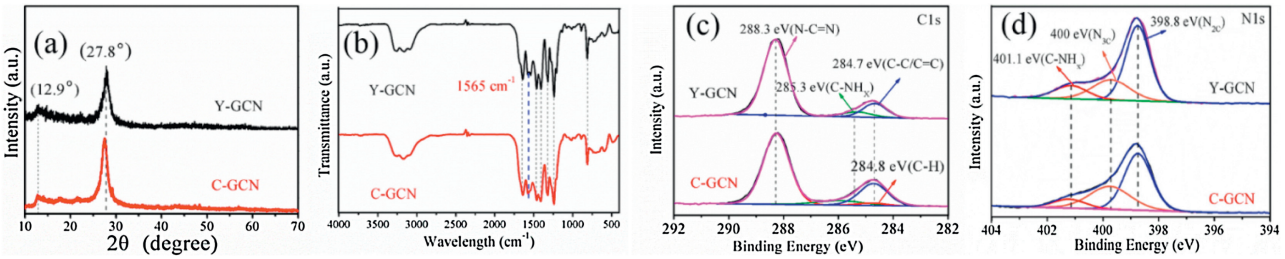

Fig. 4. XRD patterns (a) and FT-IR spectra (b) of Y-GCN and C-GCN. High-resolution XPS of spectra of C 1s (c) and N 1s (d) of Y-GCN and C-GCN.

in Figs. 5c and d, C-GCN shows more highly open-up flat and more ultrathin layered structure than Y-GCN, resulting that the surface area and pore volume of C-GCN are larger than that of the Y-GCN. As shown in Fig. S2 (Supporting information) and Table 1, the surface areas of the Y-GCN and C-GCN are 35.99 m^2/g and 79.22 m^2/g, respectively.

Thus, the results of SEM, TEM, BET, IR, XPS and NMR indicate that the calcination of urea with different kept-time can prepare g-C_3N_4 with different morphology, surface areas, polymerization's types, and molecular structure, which further lead to different photocatalytic performance of H_2 evolution. It should be noted that this is first report on polymeric carbon nitride frameworks highly relying on its precursors with different kept-time.

To explain why the reactant of urea with different kept-time lead to different structures, morphologies and photocatalytic performances of g-C_3N_4, we further investigated the precursor's nature. As shown in Fig. S3a and Table S2 (Supporting information), the results of XRD and elemental analyses show that there are no obvious difference of crystal and structure between urea-1 (the fresh urea) and urea-2 (urea kept for five years). Fig. S3b (Supporting information) shows that some differences appeared in thermal weight analysis of the two kind of precursor. There is obvious particular process among the calcination process of the urea-2 at T = 230–243 °C (process (1)) that is not exist in the calcination process of urea-1, which is ascribed to the interaction among biuret and cyanuric acid, indicating the synthetic process route of C-GCN using the urea-2 is different from that of Y-GCN using the urea-1 among thermal treatment process. The results

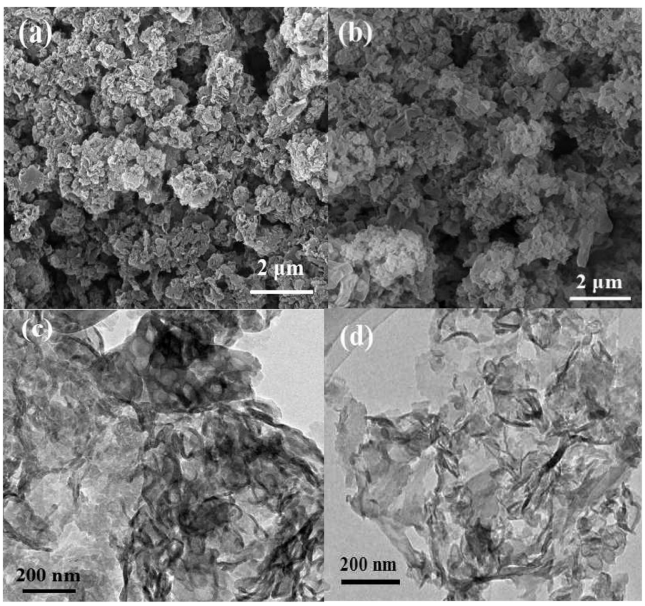

Fig. 5. SEM images of (a) Y-GCN and (b) C-GCN. TEM images of (c) Y-GCN and (d) C-GCN.

confirm that kept-time of urea can affect internal polymerization process of g-C_3N_4. Fig. S4 (Supporting information) shows that urea-2 is conglomerate and branched, while urea-1 possesses smooth rod structure, indicating different kept-time of urea make significant effect on the morphology of urea, further lead to difference in the structure and optical properties of the as-prepared g-C_3N_4. Therefore, higher photocatalytic performance of C-GCN than Y-GCN could be ascribed that differences of precursor's morphology lead to differences in specific synthetic pathways.

In order to understand the effect of terminal defects on g-C_3N_4, UV–vis diffuse reflection spectra (DRS) and Mott-Schottky plots of Y-GCN and C-GCN were investigated. As shown in Figs. 2a and b, the DRS spectra of the as prepared Y-GCN and C-GCN show that the calculated bandgaps are 2.78 and 2.66 eV for the Y-GCN and C-GCN, respectively. Figs. S5a and b (Supporting information) show the Mott-Sckottky plots of Y-GCN and C-GCN being working electrode (0.5 mol/L K_2SO_4 as electrolyte), respectively. The flat band potential (V_{fb}) as calculated from the x intercepts of the linear region are found to be –0.78 and –0.62 eV *vs.* SCE (equivalent to 0.54 and 0.38 eV *vs.* NHE, respectively) for Y-GCN and C-GCN, respectively. It is known that the flat band potential of n-type semiconductor equals to the Fermi level (EF). Therefore, the EF values of Y-GCN and C-GCN are 0.54 and 0.38 eV, respectively. Accordingly, the CB of Y-GCN and C-GCN can be calculated as –0.74 and –0.58 eV, respectively. The band positions can be calculated by the following empirical formulas: $E_{CB} = E_{VB} - E_g$, and the valence band (VB) of Y-GCN and C-GCN are 2.04 and 2.08 eV, respectively (Fig. S6 in Supporting information) [59,60]. These data suggest that the introduction of terminal —N=CH— groups into g-C_3N_4 among the C-GCN can affect the position of CB of the C-GCN, leading to the enhancement of photocatalytic performance of H_2 generation.

In order to well understand the effect of the terminal —N=CH— groups on the band structure of C-GCN, density of states (DOS) and partial density of states (PDOS) of the Y-GCN and C-GCN were performed (Fig. 6 and Fig. S6). As shown in Figs. S6a and b, both C 2p and N 2p orbitals contribute to the CB of Y-GCN, while the VB is mainly composed of C 2s and C 2p orbitals, in consistent with the previously reported results [61]. As shown in Figs. S6c and d, the CB of C-GCN is also composed of both C 2p and N 2p orbitals, whereas the VB of C-GCN is ascribed to C 2s, C 2p and N 2p orbitals. As the band alignments shown in Fig. S7 (Supporting information), the DOS shows that after introducing imine groups (—N=CH—) into the unit cell of g-C_3N_4, it narrows the band gap of g-C_3N_4 to enhance its visible light absorption, which agree well with the above results of the DRS and Mott-Sckottky plots. The results confirmed that the introduction of terminal —N=CH— groups can affect electron density, CB and VB of g-C_3N_4 in C-GCN. The analyses also confirm the difference of molecular structure, band structure and photocatalytic performance in C-GCN and Y-GCN.

Besides the above-discussed influence of functional groups of —N=CH— on the photocatalytic performance of H_2 production of g-C_3N_4, the factor of cocatalyst of Pt was systematically

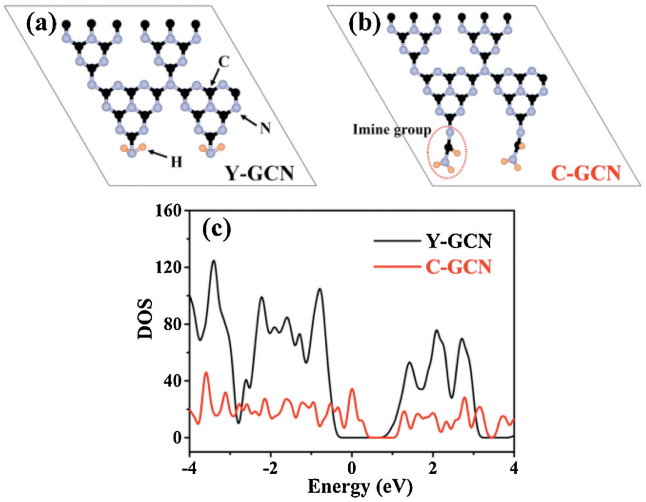

Fig. 6. Structural models of (a) Y-GCN and (b) C-GCN, respectively. (c) DOS of Y-GCN and C-GCN.

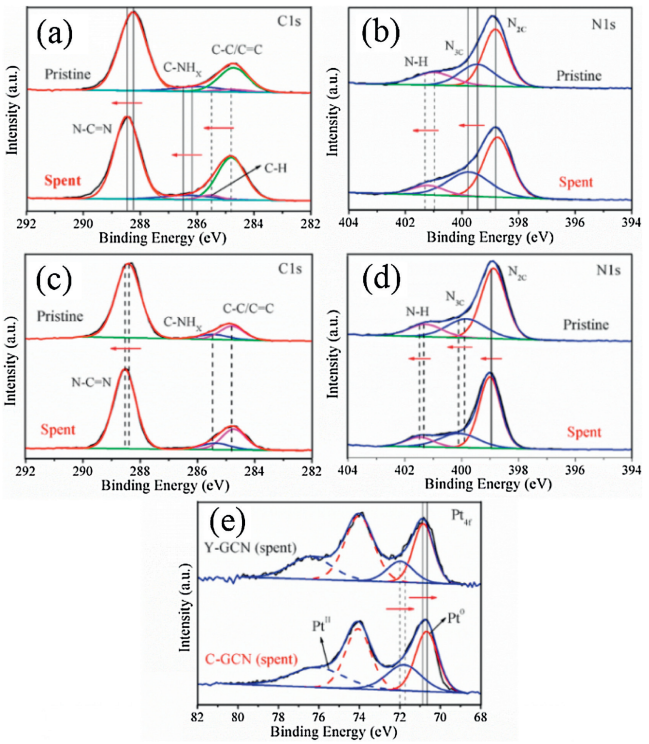

Fig. 7. (a) XPS for C 1s spectrum and (b) N 1s spectrum of the pristine C-GCN and that with *in-situ* photodeposited Pt after 20 h photocatalytic reaction. (c) XPS for C 1s spectrum and (d) N1s spectrum of the pristine Y-GCN and that with *in-situ* photodeposited Pt after 20 h photocatalytic reaction. (e) XPS of Pt on the surface of the C-GCN and Y-GCN with *in-situ* photodeposited Pt after 20 h photocatalytic reaction.

investigated. In the presence of Pt cocatalyst, the rate of H_2 production of the C-GCN is much larger than that of Y-GCN. The marked difference in photocatalytic efficiency between Y-GCN and C-GCN could arise from different transfer rates from the internal sites of the catalysts to the surface of Pt particles, depending on the coupling between active sites (—N=CH—) and Pt particles. To further explore interaction of C-GCN with Pt cocatalyst, the catalyst with *in-situ* photo deposited Pt after 20 h photocatalytic reaction was characterized by XPS and XRD. As shown in Fig. S8 (Supporting information), XRD shows the spent C-GCN has two characteristic peaks of g-C_3N_4 at 13.1° and 27.5°, while the 39.8° and 46.5° signals can be attributed to the presence of the Pt cocatalyst. The results confirm that Pt particles are successfully deposited on the surface of C-GCN, and C-GCN is very stable during the photocatalytic reaction. As shown in Figs. 7a and b, compared to the pristine C-GCN, the C1 sspectra of the spent C-GCN show three signals shifted to higher bind energy (B.E.) by over 0.3 eV, 0.3 eV and 0.7 eV for the N—C=N, C-NH_x and C—H signals, respectively. The N1 sspectra of the spent C-GCN show two signals shifted to higher B.E. by over 0.4 and 0.3 eV for the N_{3C} and N—H signals, respectively. In addition, as shown in Figs. 7c and d, compared to the pristine Y-GCN, the C1sspectra of the spent Y-GCN shows N–C=N signal shifted to higher B.E. by over 0.15 eV, while N 1s spectra of the spent Y-GCN show two signals shifted to higher B.E. by over 0.2 eV and 0.1 eV for the N_{3C} and N—H signals, respectively. After 20 h photocatalytic reaction, the B.E. value of C and N in Y-GCN and C-GCN all became larger than the pristine one, whereas there are larger shifts in the C-GCN than Y-GCN. The results indicate the electron density of C-GCN become lower than that of Y-GCN. Furthermore, as shown in Fig. 7e, the B.E. of Pt^0 on the spent C-GCN is 70.6 eV, smaller than that on the spent Y-GCN (70.9 eV). The B.E. of Pt^{II} on C-GCN (71.8 eV) is smaller than that on the spent Y-GCN (72.0 eV), which can be assigned to Pt^{2+} of PtO [62]. The directions of the shifts toward higher B.E. for the carbon and nitride and lower B.E. for Pt indicate the donation of electron density from the carbon and nitride of Y-GCN and C-GCN to Pt cocatalyst, in accord with metal-support interaction reported in the literatures [63]. But the larger shifts occurred in C-GCN than in Y-GCN, suggesting C-GCN has stronger interaction than Y-GCN with Pt cocatalyst, resulting in facilitating charge transfer and significant increase in photocatalytic hydrogen evolution. These XPS results demonstrate that the existence of —N=CH— groups in C-GCN leads to tight interaction between C-GCN and Pt nanoparticles, and then improves the charge separation and photocatalytic performance.

On the basis of the above experimental results, we proposed the mechanism of the photocatalytic hydrogen production of water splitting over the as-prepared catalysts. As shown in Scheme 1, under irradiation of visible light, C-GCN can directly absorb light of 420–520 nm to generate electrons (e^-) and holes (h^+) and the electrons are excited from VB to CB. Firstly, the photo generated electrons on the CB of the C-GCN can quickly transfer to Pt nanoparticles because there are tight interactions between C-GCN and Pt nanoparticles *via* —N=CH— groups. Meanwhile, the holes on the VB of C-GCN are reacted with the sacrificial agent of

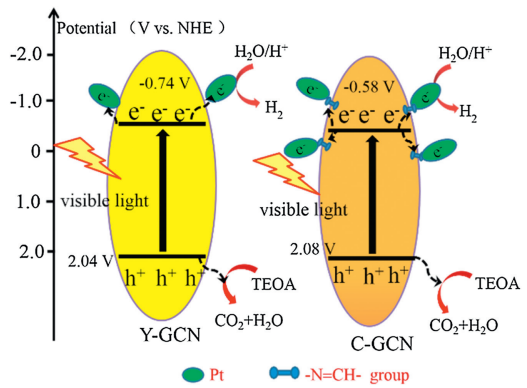

Scheme 1. Proposed photocatalytic mechanism for hydrogen evolution over C-GCN and Y-GCN under visible light irradiation.

triethanolamine to finish the oxidation process, which improves the separation of photo generated electrons and holes. Therefore, there is effective charge separation and the separated electrons have enough time to reduce H_2O to H_2 on the surface of C-GCN. As for Y-GCN, the photocatlytic mechanism is similar to that of C-GCN. But the photo-generated electrons on the CB of Y-GCN have smaller transfer rate than those on the CB of C-GCN to Pt nanoparticles because there exist functional groups of —N=CH— in C-GCN but not in Y-GCN. The mechanism explains why C-GCN exhibits much better activity for hydrogen evolution than Y-GCN.

In this paper, Y-GCN and C-GCN were firstly prepared by using the fresh urea and the urea kept for five years as precursors, respectively. The photocatalytic hydrogen evolution rate of C-GCN is much larger 5 times than that of Y-GCN. Different from Y-GCN, results of XPS, NMR, DRS indicate that there are functional groups of —N=CH— introduced in the C-GCN. Noteworthily, the introduction of functional groups of —N=CH— result in enhancement of visible light absorption, high charge-separation efficiency, suitable band structure, and strong interaction between C-GCN and Pt, and then lead to much improvement of photocatalytic activity. DFT calculation also confirms the introduction of —N=CH— can change the band structure of g-C_3N_4. The present work provides a new strategy to improve the photocatalytic performance of g-C_3N_4 *via* the introduction of functional groups of —N=CH—.

Acknowledgments

We gratefully acknowledge the financial support of the National Natural Science Foundation of China (NSFC, Nos. 51622806, 51878325, 51868050, 51378246 and 51720105001) and the Natural Science Foundation of Jiangxi Province (Nos. 20162BCB22017, 20165BCB18008, 20171ACB20017, 20133ACB21001 and 20171BAB206049).

Appendix A. Supplementary data

Supplementary material related to this article can be found, in the online version, at doi:https://doi.org/10.1016/j.cclet.2019.08.020.

References

[1] A. Fujishima, K. Honda, Nature 238 (1972) 37–38.
[2] A. Xie, Z.H. Pan, M. Yu, et al., Chin. Chem. Lett. 30 (2019) 225–228.
[3] A. Kudo, Y. Miseki, Chem. Soc. Rev. 38 (2009) 253–278.
[4] Z. Han, F. Qiu, R. Eisenberg, P.L. Holland, T.D. Krauss, Science 338 (2012) 1321–1324.
[5] Y.C. Nie, F. Yu, L.C. Wang, et al., Appl. Catal. B: Environ. 227 (2018) 312–321.
[6] Y. Wang, X. Wang, M. Antonietti, Angew. Chem. Int. Ed. 51 (2012) 68–89.
[7] J. Wang, J. Chen, P. Wang, J. Hou, C. Wang, Y. Ao, Appl. Catal. B: Environ. 239 (2018) 578–585.
[8] Y. Hou, A.B. Laursen, J. Zhang, et al., Angew. Chem. Int. Ed. 52 (2013) 3621–3625.
[9] C.C. Wang, X.H. Yi, P. Wang, Appl. Catal. B: Environ. 247 (2019) 24–48.
[10] S.Z. Wu, C.H. Chen, W.D. Zhang, Chin. Chem. Lett. 25 (2014) 1247–1251.
[11] X.H. Jiang, Q.J. Xing, X.B. Luo, et al., Appl. Catal. B: Environ. 228 (2018) 29–38.
[12] X.H. Jiang, L.C. Wang, F. Yu, J.P. Zou, et al., ACS Sustain. Chem. Eng. 6 (2018) 12695–12705.
[13] L. Jiang, X. Yuan, G. Zeng, et al., Environ. Sci. Nano 5 (2018) 599–615.
[14] H. She, Y. Sun, L. Wang, et al., Appl. Catal. B: Environ. 245 (2019) 439–447.
[15] Y.P. Wang, Y.K. Li, J.L. Zhao, et al., Int. J. Hydrogen Energy 44 (2019) 618–628.
[16] J.P. Zou, D.D. Wu, J. Luo, et al., ACS Catal. 6 (2016) 6861–6867.
[17] J.P. Zou, Y. Chen, S.-S. Liu, et al., Water Res. 150 (2019) 330–339.
[18] K. Maeda, X. Wang, Y. Nishihara, et al., J. Phys. Chem. C 113 (2009) 4940–4947.
[19] X. Wang, K. Maeda, A. Thomas, et al., Nat. Mater. 8 (2009) 76–80.
[20] J. Low, S. Cao, J. Yu, S. Wageh, Chem. Commun. 50 (2014) 10768–10777.
[21] Q. Su, J. Sun, J. Wang, et al., Catal. Sci. Technol. 4 (2014) 1556–1562.
[22] M. Ding, J.J. Zhou, H.C. Yang, et al., Chin. Chem. Lett. 31 (2020) 71-76.
[23] Y. Zhang, H. Zhang, L. Cheng, et al., RSC Adv. 6 (2016) 14002–14008.
[24] Z. Zhou, J. Wang, J. Yu, et al., J. Am. Chem. Soc. 137 (2015) 2179–2182.
[25] H.S. Zhai, L. Cao, X.H. Xia, Chin. Chem. Lett. 24 (2013) 103–106.
[26] Q. Liu, D.B. Zhu, M.L. Guo, et al., Chin. Chem. Lett. 30 (2019) 1639–1642.
[27] D.J. Martin, K. Qiu, S.A. Shevlin, et al., Angew. Chem. Int. Ed. 53 (2014) 9240–9245.
[28] Y.S. Jun, J. Park, S.U. Lee, et al., Angew. Chem. Int. Ed. 125 (2013) 11289–11293.
[29] F. Dong, Z. Wang, H. Zhang, et al., J. Colloid. Interf. Sci. 401 (2013) 70–79.
[30] J. Xu, L. Zhang, R. Shi, Y. Zhu, J. Mater. Chem. A 1 (2013) 14766–14772.
[31] T. Wu, P. Wang, J. Qian, et al., Dalton Trans. 46 (2017) 13793–13801.
[32] J. Ran, T.Y. Ma, G. Gao, et al., Energy Environ. Sci. 8 (2015) 3708–3717.
[33] J. Zhang, M. Zhang, C. Yang, X. Wang, Adv. Mater. 26 (2014) 4121–4126.
[34] Y.P. Zhu, T.Z. Ren, Z.Y. Yuan, ACS Appl. Mater. Inter. 7 (2015) 16850–16856.
[35] T. Sano, S. Tsutsui, K. Koike, et al., J. Mater. Chem. A 1 (2013) 6489–6496.
[36] X. Du, G. Zou, Z. Wang, X. Wang, Nanoscale 7 (2015) 8701–8706.
[37] H. Yu, R. Shi, Y. Zhao, et al., Adv. Mater. 29 (2017) 160548.
[38] V.W. Lau, V.W. Yu, F. Ehrat, et al., Adv. Energy Mater. 7 (2017) 1602251.
[39] J. Ran, T.Y. Ma, G. Gao, et al., Energy Environ. Sci. 8 (2015) 3708–3717.
[40] C. Zhou, R. Shi, T. Zhang, et al., Nano Res. 11 (2018) 3462–3468.
[41] Y. Cui, Z. Ding, X. Fu, X. Wang, Angew. Chem. Int. Ed. 51 (2012) 11814–11818.
[42] X. Guan, Y. Ma, H. Li, et al., J. Am. Chem. Soc. 140 (2018) 4494–4498.
[43] S.J. Makowski, P. Köstler, W. Schnick, Chem. Eur. J. 18 (2012) 3248–3257.
[44] F. Dong, L. Wu, Y. Sun, et al., J. Mater. Chem. 21 (2011) 15171–15174.
[45] Z. Zhang, K. Leinenweber, M. Bauer, et al., J. Am. Chem. Soc. 123 (2001) 7788–7796.
[46] D.T. Vodak, K. Kim, L. Iordanidis, et al., Chem.-Eur. J. 9 (2003) 4197–4201.
[47] J.P. Zou, L.C. Wang, J. Luo, et al., Appl. Catal. B: Environ. 193 (2016) 103–109.
[48] J. Zhang, F. Guo, X. Wang, Adv. Funct. Mater. 23 (2013) 3008–3014.
[49] S. Yan, Z. Li, Z. Zou, Langmuir 25 (2009) 10397–10401.
[50] H. Zhao, X. Ding, C. Wang, et al., Sci. Bull. 62 (2017) 602–609.
[51] A. Halder, S. Karak, M. Addicoat, et al., Angew. Chem. Int. Ed. 130 (2018) 5899–5904.
[52] H. Yu, R. Shi, T. Zhang, et al., Adv. Mater. 29 (2017) 1605148.
[53] N. Boonprakob, N. Wetchakun, S. Phanichphant, et al., J. Colloid. Interf. Sci. 417 (2014) 402–409.
[54] X. Zhou, F. Peng, H. Wang, et al., Chem. Commun. 47 (2011) 10323–10325.
[55] V. Štengl, S. Bakardjieva, T.M. Grygar, et al., Chem. Cent. J. 7 (2013) 41–42.
[56] H. Wang, X. Yuan, Y. Wu, et al., Appl. Catal. B: Environ. 174 (2015) 445–454.
[57] W. Yan, Y. Yu, K. Ding, et al., Solar RRL 2 (2018) 1800058.
[58] M.S. Lee, D.R. Whang, H.J. Choi, et al., Carbon 122 (2017) 515–523.
[59] J.P. Zou, S.L. Luo, L.Z. Zhang, et al., Appl. Catal. B: Environ. 140 (2013) 608–618.
[60] J. Ding, Z. Dai, F. Qin, et al., Appl. Catal. B: Environ. 205 (2017) 281–291.
[61] G. Dong, K. Zhao, L. Zhang, Chem. Commun. 48 (2012) 6178–6180.
[62] F. Fina, H. Menard, J.T. Irvine, Phys. Chem. Chem. Phys. 17 (2015) 13929–13936.
[63] P. Bera, K. Priolkar, A. Gayen, et al., Chem. Mater. 15 (2003) 2049–2060.